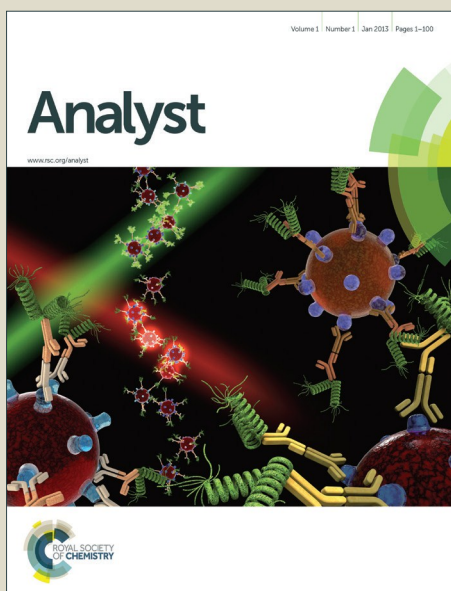


Analyst

Accepted Manuscript



This is an *Accepted Manuscript*, which has been through the Royal Society of Chemistry peer review process and has been accepted for publication.

Accepted Manuscripts are published online shortly after acceptance, before technical editing, formatting and proof reading. Using this free service, authors can make their results available to the community, in citable form, before we publish the edited article. We will replace this *Accepted Manuscript* with the edited and formatted *Advance Article* as soon as it is available.

You can find more information about *Accepted Manuscripts* in the [Information for Authors](#).

Please note that technical editing may introduce minor changes to the text and/or graphics, which may alter content. The journal's standard [Terms & Conditions](#) and the [Ethical guidelines](#) still apply. In no event shall the Royal Society of Chemistry be held responsible for any errors or omissions in this *Accepted Manuscript* or any consequences arising from the use of any information it contains.

ARTICLE

Laser-Assisted Photothermal Heating of a Plasmonic Nanoparticle-Suspended Droplet in a Microchannel

Cite this: DOI: 10.1039/x0xx00000x

T. Walsh,^a J. Lee^b and K. Park^c,

Received 00th January 2012,
Accepted 00th January 2012

DOI: 10.1039/x0xx00000x

www.rsc.org/

The present article reports the numerical and experimental investigations on the laser-assisted photothermal heating of a nanoliter-size droplet in a microchannel when plasmonic particles are suspended in the droplet. Plasmonic nanoparticles exhibit strong light absorption and scattering upon the excitation of localized surface plasmons (LSPs), resulting in intense and rapid photothermal heating in a microchannel. Computational models are implemented to theoretically verify the photothermal behavior of gold nanoshell (GNS) and gold nanorod (GNR) particles suspended in a liquid microdroplet. Experiments were conducted to demonstrate a rapid heating of a sub-100 nL droplet up to 100 °C with high controllability and repeatability. The heating and cooling time to the steady state is in the order of 1 second, while cooling requires less time than heating. The effects of core parameters, such as nanoparticle structure, volumetric concentration, microchannel depth, and laser power density on the heating are studied. The obtained results can be integrated into existing microfluidic technologies that demand accurate and rapid heating of microdroplets in a microchannel.

Introduction

Lab-on-a-chip (LOC) technology may be the most promising microfluidic research area that has enabled the integration of various physical, chemical, and biomedical laboratory operations in a single chip of a few square inches in size.¹ In particular, since LOC devices need an extremely small sample volume for the analysis and thus guarantee fast analysis and response time, significant efforts have been made to realize the LOC of biomedical diagnostics. Examples of this endeavor include temperature gradient focusing,² protein crystallization,³ solution mixing,⁴ drug discovery,⁵ and the microfluidic polymerase chain reaction (PCR).^{6,7,8} While many LOC techniques often involve local heating and cooling steps to

achieve their purposes, most of microfluidic heating systems to date have an embedded electric heater on the channel surface, heating a significant portion of the chip instead of directly heating an analyte inside the microchannel.^{1,8} This nonlocal surface heating scheme is undesirable for rapid and uniform thermal cycling, particularly when it involves a thermal cycling of microdroplets dispensed in the channel. Although recent advances have been made in microdroplet generation, dispensing, and sorting techniques to further improve a throughput and efficiency of microfluidic procedures,⁹ heating and cooling of microdroplets still rely on the electrical surface heating. Direct temperature measurement of individual droplets is another challenging issue related with microdroplet heating.

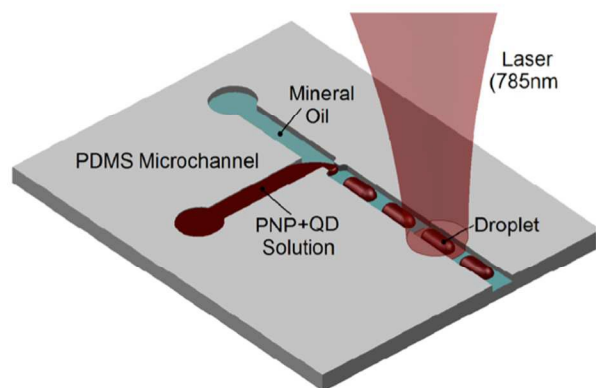


Figure 1. Schematics of heating PNP-suspended microdroplets with a laser.

This article aims to theoretically and experimentally investigate the laser-assisted photothermal heating of a plasmonic nanoparticle (PNP)-suspended liquid droplet in a microchannel. Figure 1 schematically illustrates the laser-assisted heating of PNP-suspended droplets, where droplets are generated by a T-junction microchannel¹⁰ and illuminated by a laser. The photothermal heating has been demonstrated as an effective, direct heating method of liquid samples.^{7,11,12} However, most of the previous works have focused on relatively large liquid samples or droplets that were not small enough to be deliverable through microchannels. Photothermal heating of droplets in a microchannel requires stronger light absorption across the channel depth typically in the order of hundred micrometers or smaller. The present study addresses this challenge by exciting the localized surface plasmons (LSPs) at plasmonic nanoparticles dispersed in a droplet. It has been revealed that when the LSP is excited, a significant portion of incoming photon energy is resonantly absorbed to induce a collective oscillation of free electrons confined in each PNP, leading to effective local heating of nanoparticles and surroundings.^{8,13} In the following sections, we numerically and experimentally demonstrate that this plasmonic light absorption is strong enough to enable the local heating of microdroplets in a microchannel. Two gold nanoparticle geometries – silica-core gold nanoshells (GNSs) and gold nanorods (GNRs) were considered as suspended PNPs in the present study, as they are commercially available nanostructures that provide tunability of the LSP excitation wavelength to the near-infrared region.^{12,13} The effects of a PNP concentration, microchannel depth, and laser power density on the heating process are discussed as well. Transient heating experiments were also conducted to show that the microdroplet can be rapidly heated to a sub-boiling temperature slightly less than 100°C with full heating and cooling time in the order of 1 second.

Numerical Study

In order to examine the feasibility of the LSP-mediated photothermal heating, the light absorption/scattering coefficients and the associated photothermal energy absorption depth of GNS and GNR liquid suspensions were numerically calculated. The light absorption/scattering coefficients of the GNS-suspended liquid was calculated using the Mie scattering theory.¹⁴ The absorption and scattering coefficients of the GNS-suspended liquid, i.e., α_λ and σ_λ , can be written as

$$\alpha_\lambda = (1-f)\alpha_{w,\lambda} + \frac{3f}{2D}Q_{a,\lambda}$$

$$\sigma_\lambda = \frac{3f}{2D}Q_{s,\lambda}$$
(1)

where $\alpha_{w,\lambda}$ is the absorption coefficient of water, and D and f is the diameter and the volume fraction of the GNS particles, respectively. $Q_{a,\lambda}$ and $Q_{s,\lambda}$ are the absorption and scattering efficiencies of single GNS particle that can be calculated from the Mie scattering. It should be noted that Eq. (1) is valid when the particle volume fraction is very low, less than approximately 0.6%, with a small particle size parameter (i.e., $\pi D/\lambda < 1$, where λ is the wavelength of the incidence light).¹⁵ Our experimental conditions were in the range of particle

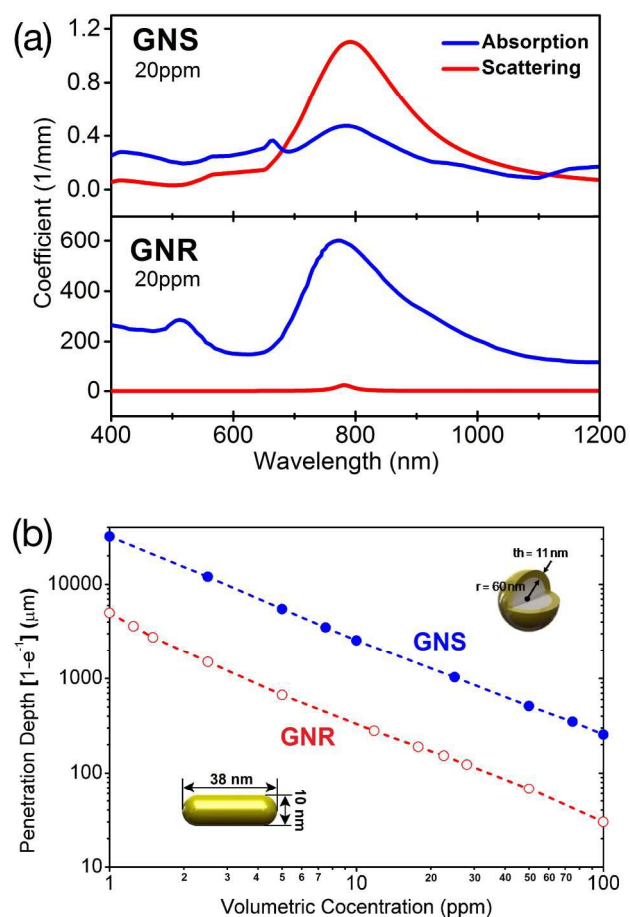


Figure 2. (a) Calculated effective absorption and scattering coefficients of GNS and GNR geometries at 20 ppm. (b) Calculated penetration depth of 785nm laser spectrum for varying GNR and GNS concentrations.

1 volume fractions less than 100 ppm (or 0.1%) and used GNS
 2 particles with a small particles size parameter (i.e.,
 3 $\pi D / \lambda = 0.57$), which satisfies the valid limit of Eq. (1). To
 4 consider the broadening of the plasmonic effect when the
 5 nanoparticle sizes are smaller than the mean free path of the
 6 conduction electrons, the size-dependent dielectric function of
 7 gold was calculated using the Drude model with modified
 8 scattering rate.¹⁶ Figure 2a shows the calculated absorption and
 9 scattering coefficients of a GNS-suspended liquid when its
 10 volumetric concentration is 20 ppm, and the GNS geometry is
 11 120 nm in diameter for a silica core and 11 nm for the gold
 12 layer thickness. It is apparent that the considered GNS
 13 geometry excites the LSP to provide absorption and scattering
 14 peaks at 785 nm. However, the GNS has stronger light
 15 scattering than absorption upon the LSP excitation,
 16 substantially affecting the overall photothermal absorption of
 17 incident light. Light scattering should be taken into account to
 18 calculate the volumetric photothermal absorption rate of the
 19 GNS-nanofluid.

20
 21 Since the Mie scattering theory cannot be directly used for
 22 the GNR structure due to its high aspect ratio rod geometry, the
 23 present study used the boundary element method (BEM)¹⁷ to
 24 determine the effective light absorption/scattering coefficients
 25 of a GNR-suspended liquid. The BEM solves three-dimensional
 26 Maxwell's equations in the presence of arbitrarily shaped
 27 dielectrics by expressing them as the self-consistent surface-
 28 integral equations with interface charges and currents. When
 29 compared with other numerical methods, such as the discrete
 30 dipole¹⁸ and multiple motipole¹⁹ approximations, the finite
 31 difference time domain method,²⁰ and the dyadic Green
 32 function technique,²¹ the BEM discretizes only the boundaries
 33 between the different dielectric materials, not the whole
 34 volume, and thus provides faster simulations with moderate
 35 memory requirements. Particularly, the BEM is advantageous
 36 in simulating three-dimensional plasmonic materials due to its
 37 capability of describing metals with thin skin depths and high
 38 dielectric contrast while exhibiting fast convergence. Since
 39 GNRs are dispersed in a liquid in random orientations, the
 40 effective absorption/scattering coefficients were calculated by
 41 taking the average of the absorption/scattering coefficients for
 42 different GNR orientations relative to the direction of incident
 43 light. Figure 2a also shows the effective light absorption and
 44 scattering coefficients of a GNR-suspended liquid when its
 45 concentration is 20 ppm, and the GNR geometry is 38 nm in
 46 length and 10 nm in diameter. For the given geometry, there is
 47 a light absorption peak at 785 nm due to the LSP excitation
 48 along the long axis of the GNR. The absorption peak value is
 49 around three orders of magnitude stronger than the GNS at the
 50 same concentration, indicating that the LSP at the GNR induces
 51 a much stronger electromagnetic field in proximity to its
 52 interface. Compared to light absorption, light scattering of the
 53 GNR is negligibly small and can be ignored when the
 54 photothermal absorption rate of the GNR-suspended liquid is
 55 calculated.
 56
 57
 58
 59
 60

Once the light absorption/scattering coefficients are determined, we can calculate the volumetric photothermal absorption rate by solving the radiative transport equation:¹⁵

$$\frac{dI_\lambda}{ds} = -(\alpha_\lambda + \sigma_\lambda)I_\lambda + \frac{\sigma_\lambda}{4\pi} \int_{4\pi} I_\lambda(\hat{s}_i)\Phi(\hat{s};\hat{s}_i)d\Omega_i \quad (2)$$

where I_λ is the spectral intensity of the laser, α_λ is the spectral absorption coefficient, σ_λ is the spectral scattering coefficient, Ω_i is the solid angle of the beam, and Φ is the in-scattering probability to the solid angle Ω_i about the direction \hat{s} . It should be noted that the second term of Eq. (2) is associated with the in-scattering augmentation of the light intensity and should be calculated when the scattering coefficient is comparable to the absorption coefficient (i.e., the GNS solution). However, since it is challenging to determine the in-scattering probability, the present study employed a Monte Carlo simulation to stochastically trace the scattering and absorption of 20 million photons per wavelength upon colliding with randomly dispersed GNSs.¹⁶ From the Monte Carlo simulation, the ensemble-averaged spectral intensity distribution $\langle I_\lambda(z) \rangle$ can be determined as a function of the depth to the solution. When compared to the GNS case, the computation of the GNR case is straightforward. Since light scattering can be ignored, the spectral intensity distribution can be approximated as $I_\lambda(z) = I_\lambda^0 e^{-\alpha_\lambda z}$, where I_λ^0 is the incident spectral intensity, from the Beer-Lambert law.²² The computation results are shown in Figure 2b in terms of the penetration depth as a function of nanoparticle volumetric concentration. The penetration depth is defined as the depth required to absorb 63.2 % (or $1 - e^{-1}$) of incident light. When plotted on a log-log scale, the penetration depth almost linearly decreases for a wide range of the volumetric concentration for both nanoparticles. However, the GNR has an approximately one order of magnitude smaller penetration depth than the GNS, indicating that the GNR is a better photothermal energy absorber. The penetration depth of the GNR solution is on the order of 100 μm for its commercially available concentration range at around 10 ppm, which would allow substantial photothermal energy absorption across a typical microchannel depth. The consequent temperature distribution of a PNF microdroplet surrounded by mineral oil in a microchannel was also calculated and discussed in the Supporting Information.

Experimental Study

Experimental setup

Based on the computation results, the plasmonic photothermal heating for a microdroplet-in-microchannel configuration was experimentally investigated. As shown in Fig. 3a, the experimental setup was established with an inverted microscope (Olympus IX-71) having two light sources for fluorescence and LSP excitation. For the fluorescence excitation light source, a mercury-vapor arc lamp was installed along with a transmission filter having a 460-500 nm

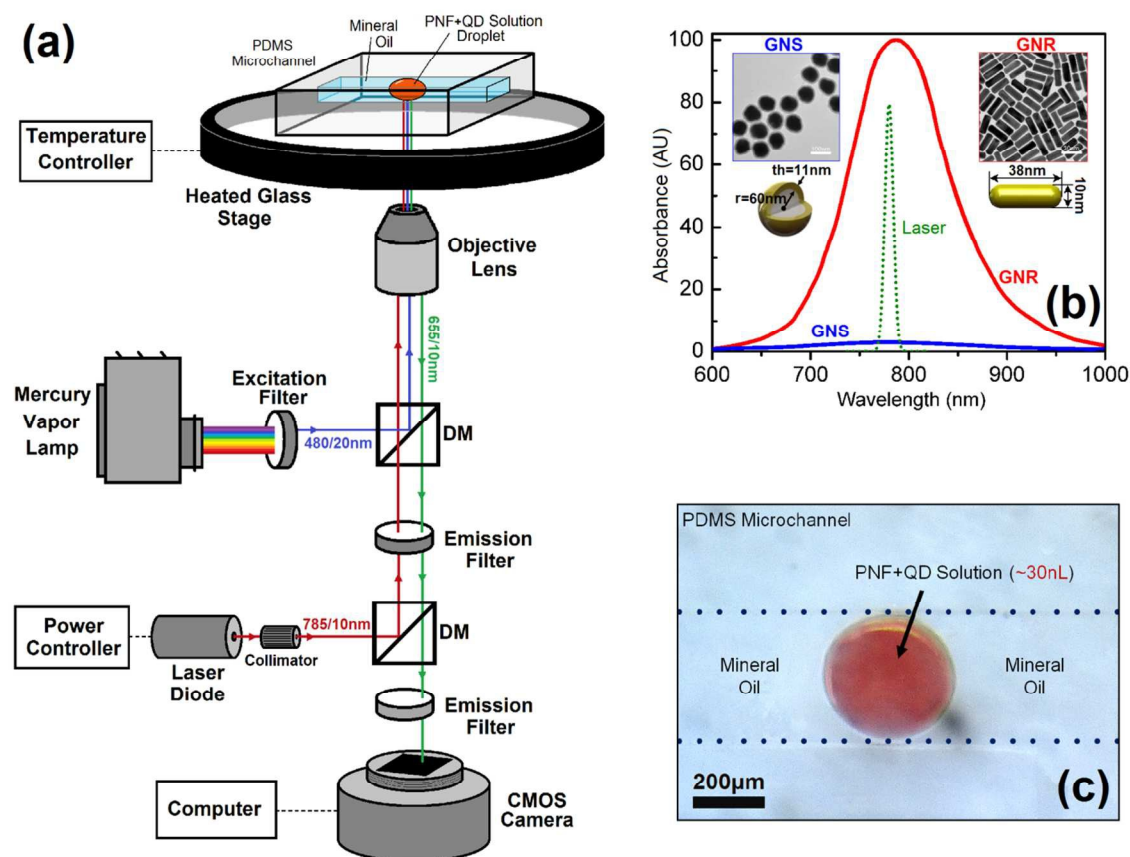


Figure 3. (a) Measured optical density spectrum for the undiluted GNS and GNR solutions with corresponding nanoparticle structures and TEM images. TEM scale-bar: (GNS) 100nm, (GNR) 30nm. (b) Combined schematic for fluorescence-temperature relation and laser heating experimental setup. (c) Microscope image of a microdroplet inside of microchannel.

bandwidth. On the other hand, the LSP excitation light source was realized with a power-controllable, continuous-wave (CW) fiber optic laser whose wavelength is 785 nm with a 10-nm sharpness (B&W Tek). The fiber laser with a beam collimator produces a beam waist of ~ 2.2 mm before focusing. The beam was slightly unfocused to provide more uniform heating of a droplet. The beam diameter onto the droplet was estimated to be ~ 500 μm , which was large enough to illuminate the whole droplet in the microchannel. For nanoparticles, 60/11-nm silica-core GNS (Nanospectra) and 10/38-nm GNR (Nanopartz) aqueous solutions were purchased and prepared for the experiment. Figure 3b shows the measured absorbances and TEM images of the GNS and GNR solutions when their concentrations are $\sim 1 \times 10^{10}$ cm^{-3} (or 0.5 ppm) and $\sim 8 \times 10^{13}$ cm^{-3} (or 23 ppm), respectively. While both nanoparticle solutions have a peak at ~ 780 nm, the GNR solution has a ~ 30 times stronger absorbance peak than the GNS solution. For the temperature measurement of a microdroplet, the present study chose the fluorescence thermometry²³ using CdSe/ZnS quantum dots (QDs) with the emission wavelength of 655 nm (Invitrogen, Qdot655). QDs were chosen over conventional fluorophores (e.g., Rhodamine B) for fluorescence thermometry due to the strong resistance of QDs to photobleaching.²⁴ Photobleaching is an undesirable phenomenon for fluorescence

thermometry particularly when it is related with longer periods of photothermal heating using a high power laser. Moreover, fluorescence quantum yield of QDs is much higher than that of conventional fluorophores, which is beneficial for the temperature measurement of small droplet volumes. It should be noted that the QDs for fluorescence thermometry were carefully selected to have fluorescence (at 655 nm) off the plasmon wavelength of the GNS/GNR at 780 nm, preventing possible optical coupling between the QD emission and the LSP excitation. The previous studies have revealed that QD fluorescence is greatly affected by the presence of LSPs when they are spectrally coupled.²⁵ In the experimental setup, fluorescence emission light from QDs is collected and filtered to transmit the wavelength band from 610 to 657 nm to a 1.3 MP CMOS camera.

PNP/QD solution preparation

PNP/QD solutions were carefully prepared to produce well dispersed nanoparticle suspension through the following steps: the gold nanoparticle solutions were first sonicated for 30 minutes at 37 kHz and 120 W power and diluted to several concentrations with a magnetic stirring step. Borosilicate was then added to the solution to match its pH value with that of the QD solution at pH = 9. The pH-value matching is necessary to

Lab Chip

stabilize the nanoparticle solution by preventing agglomerations and varied fluorescent properties of the QDs. After mixing, PNP/QD solutions were sonicated again for 30 minutes at 37 kHz and 120 W power prior to experiments. For the best sensitivity in fluorescence thermometry, the QD volumetric concentration was maintained at $\sim 1 \times 10^8 \text{ cm}^{-3}$ for all nanoparticle concentrations.

Fabrication of microchannel

A soft lithography procedure was carried out for the fabrication of the PDMS microchannels. The Si wafer mold was first silanized with (tridecafluoro-1,1,2,2-tetrahydrooctyl)-1-trichlorosilane for 1 hr under vacuum in order to facilitate the release of the cured PDMS pattern. A PDMS prepolymer (sylgard 184) and curing agent were purchased from Dow Chemical, thoroughly combined (wt:wt=10:1), thinly applied over the SI wafer mold, degassed in a vacuum, and cured at 60°C for 2 hrs. The fully cured PDMS microchannel surfaces were oxidized with an O₂ plasma asher to facilitate bounding and to make the channel walls hydrophilic, followed by the cleaning process of the microchannel by flushing with isopropyl alcohol. For microfluidic experiments, a T-junction microchannel pattern was fabricated to have a channel depth of 150 μm and a width of 400 μm.

Injection of PNP/QD microdroplets into a microchannel

PNP/QD microdroplets were generated by injecting a PNP/QD solution and mineral oil USP to each inlet of the T-junction microchannel with an automated syringe pump. By adjusting the injecting rates of these immiscible fluids, the volume and interval of PNP/QD droplets can be precisely controlled.¹⁰ Figure 3c shows an example of a generated microdroplet having $\sim 30 \text{ nL}$ in volume (or $\sim 190 \text{ μm}$ in radius). To achieve this, an injection rate of $0.1 \text{ μL} \cdot \text{min}^{-1}$ and $0.06 \text{ μL} \cdot \text{min}^{-1}$ was selected for the mineral oil and PNP/QD fluids, respectively. Once generated, the PNP/QD microdroplets were pushed through the microchannel strait close to the laser-illuminating spot, and the syringe pump was stopped to allow the droplet to settle and finally stop in the channel. The position of the stationary droplet was then re-aligned to the laser spot for the laser-heating experiment. The flow rate of the droplet was $\sim 5 \text{ μm/s}$, slow enough to cause negligible dynamic effect on the droplet during its delivery to the laser spot.

Results and Discussion

Fluorescence thermometry calibration

For fluorescence thermometry of a microdroplet during the photothermal heating, the temperature dependence of the fluorescence intensity should be calibrated for different concentrations of nanoparticle suspensions. To this end, a hemispherical PNP/QD droplet surrounded by mineral oil USP was formed in direct contact with an indium tin oxide (ITO) heater plate to minimize the temperature offset between the heater and the droplet. The heater plate was interfaced with a

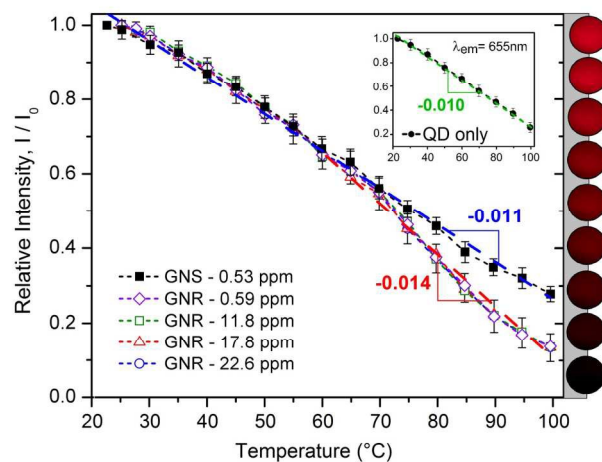


Figure 4. Relative fluorescence intensity change of each PNP+QD solution droplet as a function of temperature. Right-hand axis depicts actual microscope images of the corresponding left-hand axis values. Inlay shows the temperature-fluorescence intensity change of a droplet with only the QD solution.

temperature controller (Bioscience Tools) to control the droplet temperature with a $\pm 0.1 \text{ °C}$ precision. While changing the heater temperature from room temperature to 100°C, the QD fluorescence was measured with the CMOS camera and post-processed to obtain the pixel-averaged brightness and normalized with the initial fluorescence brightness measured at room temperature (22°C).

Figure 4 shows the normalized fluorescence intensities of GNS/QD and GNR/QD solutions as a function of temperature. The circular images at the right y-axis are real fluorescence images of a GNR/QD droplet when the volumetric concentration of GNRs is 22.6 ppm. The QD fluorescence intensities for both nanofluids linearly decrease with temperature, consistently with the previous results.^{23,24,26} This linear temperature dependence is more desirable for fluorescence thermometry than conventional fluorophores that have a complicated non-linear temperature dependence.²⁷ For the GNS solution, the temperature sensitivity is estimated to be -0.011 °C^{-1} over the temperature range of our interest, which is slightly steeper than -0.010 °C^{-1} without nanoparticles shown in the inset. On the other hand, the GNR solutions show a bilinear temperature dependence; the temperature sensitivity is almost the same as that of the GNS nanofluid up to $\sim 60 \text{ °C}$, but becomes steeper to -0.014 °C^{-1} as temperature further increases. This observation indicates that the presence of plasmonic nanoparticles influences the temperature-dependence of QD fluorescence presumably due to near-field electromagnetic interactions, such as Förster resonance energy transfer,²⁸ between the gold nanoparticles and the QDs upon LSP excitation. However, the slope of QD fluorescence remains nearly identical for different GNR concentrations, suggesting that the volumetric concentration of the nanoparticles makes very little effect on the temperature-dependence of QD fluorescence within the concentration range of practical use. The temperature resolution for both GNS/QD and GNR/QD

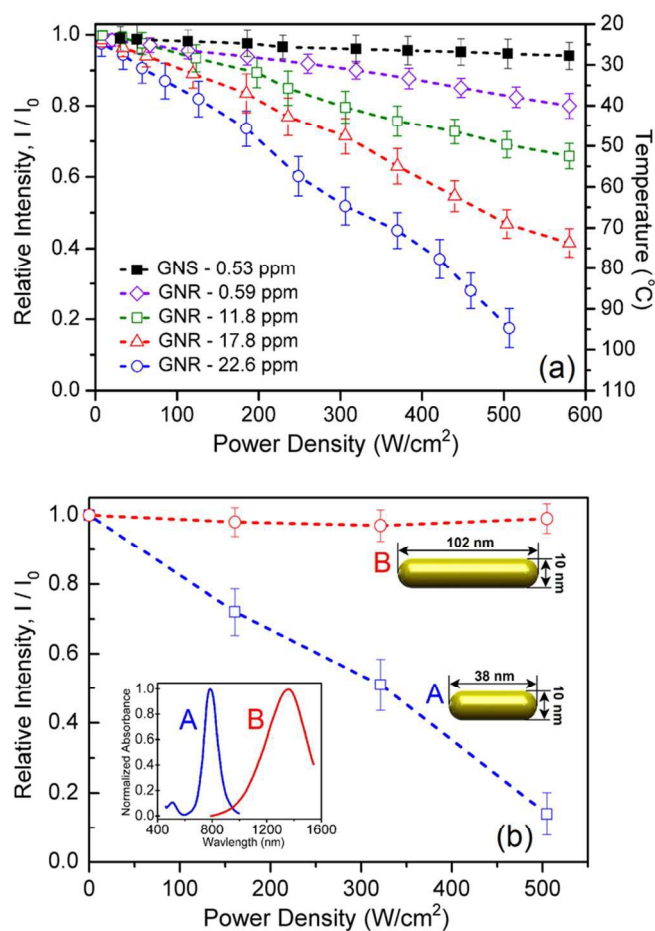


Figure 5. (a) Relative intensity of fluorescence emission versus microdroplet temperature. Right-hand axis is a visual representation of the relative intensity change for QD emission at 655nm wavelength. (b) Relative intensity of fluorescence emission versus laser excitation power density for PNF-QD solution of 2 varying GNR structures. A: 38/10-nm GNR with LSPR at 780nm, B: 102/10-nm GNR with LSPR at 1400 nm.

cases is commonly ± 1 °C, which are in the same order as the previous results.^{24,27}

Plasmonic photothermal heating

With the fluorescence calibration results for GNS/QD and GNR/QD suspensions, the laser-assisted photothermal experiment was conducted for a PNP droplet in a PDMS microchannel. While the 785-nm laser beam was illuminated onto a single stationary droplet through a slightly unfocused $10\times$ objective lens, the QD fluorescence images were recorded with the mounted CMOS camera. These images were collected across the adjustable power density range of the laser, post-processed to obtain the pixel-averaged brightness, and were then normalized with respect to the initial brightness prior to laser heating. Figure 5a shows the steady-state photothermal heating results of GNS/QD and GNR/QD microdroplets as a function of the input laser power density. The steady-state QD fluorescence was measured after 5 min upon increasing the laser power density, which is enough time to achieve the steady

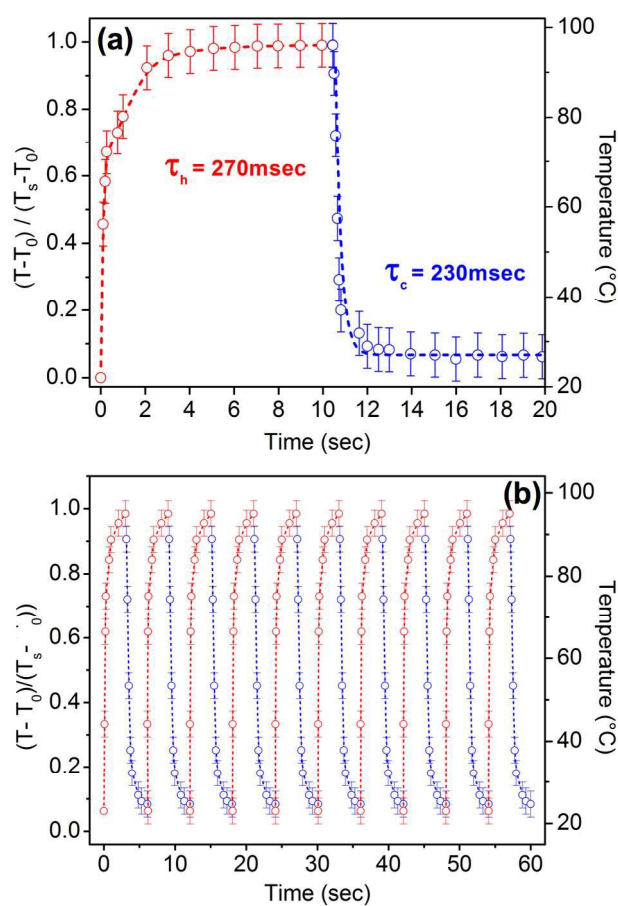


Figure 6. (a) Normalized full transient temperature response of GNR/QD droplet from 0 to $500 \text{ W}\cdot\text{cm}^{-2}$ laser power. The red dashed line shows the droplet heating and thermal time constant. The blue dashed line shows the cooling of the droplet and thermal time constant. (b) Temporal continuation of normalized full transient temperature response from 0 to $500 \text{ W}\cdot\text{cm}^{-2}$ laser power through 10 heating and cooling cycles of the GNR/QD droplet.

state as will be shown in the transient analysis. For a GNS droplet, its maximum concentration is 0.53 ppm after mixing with a QD solution, only able to reach ~ 26 °C (or $\Delta T = \sim 5$ °C) at the laser power density of $550 \text{ W}\cdot\text{cm}^{-2}$. It should be noted that this GNS concentration was the maximum of commercial GNS samples. When the GNR solution was examined for different GNR concentrations (i.e., 0.59, 11.8, 17.8, and 22.6 ppm), the photothermal heating was observed to be more prominent; the GNR concentration of 22.6 ppm increases the microdroplet temperature up to ~ 100 °C with the laser power density of $500 \text{ W}\cdot\text{cm}^{-2}$. The absorbed laser power by the nanorod-suspended microdroplet ($\sim 190 \mu\text{m}$ in radius and 22.6 ppm in nanorod concentration) estimated to be ~ 35 mW. It should be noted that further photothermal heating was possible to induce droplet boiling, but we only focused on the sub-boiling heating of a droplet in this paper. Even the lowest concentration of the GNR mixture (0.59 ppm) generates a ~ 15 °C higher temperature rise than the GNS mixture of nearly the same volumetric concentration (0.56 ppm). This strongly suggests that GNR structures would serve optimally for smaller

1 microdroplets where the absorption efficiency becomes more
2 important. In order to verify that the observed photothermal
3 heating is mainly due to the plasmonic excitation, two GNR
4 structures with different LSP excitation wavelengths were
5 illuminated with a 785-nm laser. As shown in Fig. 5b, GNR A
6 that has the absorption peak at ~ 1400 nm exhibits very little
7 change in its fluorescence when illuminated with the laser.
8 However, GNR B demonstrates a clear temperature increase
9 under the same condition, indicating that the LSP excitation
10 effectively converts the incident photon energy to thermal
11 energy.

12
13 The transient response of the laser-assisted droplet heating
14 plays an imperative role in achieving a rapid and repeatable
15 thermal cycling in photothermal microfluidic systems. Figure
16 6a shows the transient temperature changes of a ~ 30 nL GNR
17 microdroplet with the volumetric concentration of 22.6 ppm
18 during a laser heating and cooling. The laser power density was
19 switched on from 0 to $500 \text{ W}\cdot\text{cm}^{-2}$ for 10 seconds and switched
20 off during the transient experiment. From the obtained thermal
21 cycling plot, the heating time to the steady state is estimated to
22 approximately 3 seconds while the cooling time is
23 approximately 1 second. The faster cooling time is most likely
24 attributed to the heat conduction loss to the surrounding
25 medium as a result of the large surface/volume ratio of the
26 microdroplet. When the thermal time constant is conventionally
27 defined as time taken for the droplet temperature to reach
28 63.2% (or $1 - e^{-1}$) of the steady value, the heating and cooling
29 thermal time constants are similar to be 270 msec and 230
30 msec, respectively. From the thermal time constant estimation,
31 the effective thermal transient rate can be estimated to be
32 $240^\circ\text{C}/\text{s}$, which is a significant improvement compared to many
33 of the conventional thermoelectric systems available with a
34 maximum rate of $\sim 10^\circ\text{C}/\text{s}$.^{1,29} Figure 6b demonstrates that the
35 microdroplet heating/cooling process is fully repeatable and
36 consistent over many cycles. Since a typical microfluidic
37 heating procedure consists of a number of thermal cycles with
38 repeated heating and cooling steps, a consistent heating/cooling
39 process with high repeatability is strongly required in achieving
40 an efficient and improved throughput.

41 We occasionally observed the formation of bubbles around
42 aggregated GNRs when they are not well dispersed during the
43 rapid photothermal heating: see supplemental video 1, where
44 dark colored areas are aggregated GNRs. This bubble formation
45 may be due to localized boiling^{11,28} and/or the escape of
46 entrapped air pockets in the aggregated GNRs. This
47 phenomenon often resulted in intensive microscale
48 thermophoresis effects when the excitation power of the laser
49 reached a critical intensity, commonly inducing fluid
50 circulation, voids within the PNF, and the eventual collapse of
51 the well-formed water-oil phase boundary. Great care should be
52 taken to properly prepare the PNF solutions and control the
53 localized heating effects caused by the excitation source.
54 Another noteworthy observation was a local convection near
55 the center of the laser focal point in the droplet.³⁰ It should be
56 noted that for a ~ 30 nL microdroplet the Raleigh number is
57 estimated to be 0.08, which is small enough to ignore the

natural convection inside the droplet.²² However, we observed
convection behaviors in a ~ 30 nL droplet: see Supplemental
Video 2. We believe that convection observed in our
experiment may be caused by the inverted optical setup of the
laser illumination. The bottom center of the droplet focused by
the laser beam is locally overheated than the neighboring zone
due to the Gaussian laser beam profile, yielding a local
buoyancy force large enough to circulate the fluid in the
microdroplet. We believe that this convection promotes the
temperature uniformity of the microdroplet during the
photothermal heating.

Conclusions

The present study has theoretically and experimentally
investigated the plasmonic photothermal heating of a GNS- and
GNR-suspended microdroplet within a PDMS microchannel.
Fluorescence thermometry using CdSe/ZnS QDs was
implemented to remotely and accurately measure the
microdroplet temperature in the microchannel with the
temperature resolution of $\pm 1^\circ\text{C}$. When given the same
volumetric concentration, GNRs are significantly more
effective than GNSs for photothermal heating. At GNR
solutions of ~ 20 ppm in concentration, a laser power density of
 $\sim 500 \text{ W}\cdot\text{cm}^{-2}$ attains a full range of steady-state temperatures of
a ~ 30 nL microdroplet from room temperature to $\sim 100^\circ\text{C}$. The
transient heating and cooling behaviours of the GNR
microdroplet are very fast with the rate of $240^\circ\text{C}/\text{s}$ and highly
repeatable over numerous continuous cycles. The obtained
results viably demonstrate the potential of plasmonic
photothermal heating integrated with microfluidic systems,
which will greatly benefit existing LOC applications, such as
PCR and TGF, by enhancing the throughput and efficiency.

Acknowledgements

This work was supported by National Research Foundation
Grant funded by the Korean Government (NRF-2011-220-
D00014) and NSF (CBET-1337061 and CBET-1403072). KP
also thanks for the startup support from the University of Utah.

Notes and references

^a Department of Mechanical, Industrial and Systems Engineering,
University of Rhode Island, Kingston, RI 02881, USA.

^b Department of Mechanical Engineering, Sogang University, Seoul, 121-
742, South Korea.

^c Department of Mechanical Engineering, University of Utah, Salt Lake
City, UT 84112, USA.

E-mail: kpark@mech.utah.edu; Fax: +1 (801) 585 9826; Tel: +1 (801)
581 4260

† Electronic Supplementary Information (ESI) available: details of any
supplementary information available should be included here. See
DOI: 10.1039/b000000x/

- 1
2
3
4
5
6
7
8
9
10
11
12
13
14
15
16
17
18
19
20
21
22
23
24
25
26
27
28
29
30
31
32
33
34
35
36
37
38
39
40
41
42
43
44
45
46
47
48
49
50
51
52
53
54
55
56
57
58
59
60
- 1 C. D. Chin, V. Linder, S. K. Sia, *Lab Chip* 2007, **7**, 41; L. Y. Yeo, H. C. Chang, P. P. Y. Chan, J. R. Friend, *Small* 2011, **7**, 12; V. Miralles, A. Huerre, F. Malloggi, M. C. Jullien, *Diagnostics* 2013, **3**, 33.
- 2 T. Matsui, J. Franzke, A. Manz, D. Janasek, *Electrophoresis* 2007, **28**, 4606.
- 3 P. Laval, N. Lisai, J.B. Salmon, M. Joanicot, *Lab Chip* 2007, **7**, 829.
- 4 A. D. Stroock, S. K. W. Dertinger, A. Ajdari, I. Mezic, H. A. Stone, G. M. Whitesides, *Science* 2002, **295**, 647.
- 5 C. O. Kappe, D. Dallinger, *Nat. Rev. Drug Discov.* 2006, **5**, 51; J. T. Wang, J. Wang, J. J. Han, *Small* 2011, **7**, 1728.
- 6 J. Chiou, P. Matsudaira, A. Sonin, D. Ehrlich, *Anal. Chem.* 2001, **73**, 2018; M. Curcio, J. Roeraade, *Anal. Chem.* 2002, **75**, 1; K. Sun, A. Yamaguchi, Y. Ishida, S. Matsuo, H. Misawa, *Sens. Actuators, B* 2002, **84**, 283; ; M. Krishnan, V. M. Ugaz, M. A. Burns, *Science* 2002, **298**, 793; N. Park, S. Kim, J. H. Hahn, *Anal. Chem.* 2003, **75**, 6029; D. Braun, N. L. Goddard, A. Libchaber, *Phys. Rev. Lett.* 2004, **91**, 10; D. Braun, *Mod. Phys. Lett. B* 2004, **18**, 775; E. K. Wheeler, W. Bennett, P. Stratton, J. Richards, A. Chen, A. Christian, K. D. Ness, J. Ortega, L. G. Li, T. H. Weisgraber, K. Goodson, F. Milanovich, *Anal. Chem.* 2004, **76**, 4011; Z. Guttenberg, H. Muller, H. Habermuller, A. Geisbauer, J. Pipper, J. Felbel, M. Kielpinski, J. Scriba, A. Wixforth, *Lab Chip* 2005, **5**, 308; S. Mohr, Y. H. Zhang, A. Macaskill, P. Day, R. Barber, N. Goddard, D. Emerson, P. Fielden, *Microfluid. Nanofluid.* 2007, **3**, 611; N. R. Beer, B. J. Hindson, E. K. Wheeler, S. B. Hall, K. A. Rose, I. M. Kennedy, B.W. Colston, *Anal. Chem.* 2007, **79**, 8471; R. Dettlof, E. Yang, A. Rulison, A. Chow, J. Farinas, *Anal. Chem.* 2008, **80**, 4208; A. Reichert, J. Felbel, M. Kielpinski, M. Urban, B. Steinbrecht, T. Henkel, *J. Bionic Eng.* 2008, **5**, 291; Y. Schaeerli, R. C. Wootton, T. Robinson, V. Stein, C. Dunsby, M. A. A. Neil, P. M. W. French, A. J. deMello, C. Abell, F. Hollfelder, *Anal. Chem.* 2008, **81**, 302; M. M. Kiss, L. Ortoleva-Donnelly, N. R. Beer, J. Warner, C. G. Bailey, B. W. Colston, J. M. Rothberg, D. R. Link, J. H. Leamon, *Anal. Chem.* 2008, **80**, 8975; A.L. Markey, S. Mohr, & P.J.R. Day, *Methods* 2010, **50**, 277; Y. Schaeerli, F. Hollfelder, *Mol. Biosyst.* 2009, **5**, 1392; L. Mi, Y. Wen, D. Pan, Y. Wang, C. Fan, J. Hu, *Small* 2009, **5**, 2597.
- 7 R. P. Oda, M. A. Strausbauch, A F. R. Huhmer, N. Borson, S. R. Jurrens, J. Craighead, P. J. Wettstein, B. Eckloff, B. Kline, J. P. Landers, *Anal. Chem.* 1998, **70**, 4361; K. H. Cheong, D. K. Yi, J.-G. Lee, J.-M. Park, M. J. Kim, J. B. Edell, C. Ko, *Lab Chip* 2008, **8**, 810; H. Kim, S. Dixit, C. Green, G. Faris, *Opt. Express* 2009, **17**, 218.
- 8 Y. Zhang, P. Ozdemir, *Anal. Chem. Acta* 2009, **638**, 115.
- 9 S. Xu, Z. Nie, M. Seo, P. Lewis, E. Kumacheva, H. A. Stone, P. Garstecki, D. B. Weibel, I. Gitlin, G.M. Whitesides, *Angew. Chem.* 2005, **117**, 734; D. Dendukuri, D. C. Pregibon, J. Collins, T. A. Hatton, P. S. Doyle, *Nat. Mater.* 2006, **5**, 365; C. H. Choi, J. H. Jung, D. W. Kim, Y. M. Chung, C. S. Lee, *Lab Chip* 2008, **8**, 1544; S. E. Chung, W. Park, S. Shin, S. A. Lee, S. Kwon, *Nat. Mater.* 2008, **7**, 587; B. Laulicht, P. Cheifetz, E. Mathiowitz, A. Tripathi, *Langmuir* 2008, **24**, 9717; J. Wan, A. Bick, M. Sullivan, H. A. Stone, *Adv. Mater.* 2008, **20**, 3314; W. Li, H. H. Pham, Z. Nie, B. MacDonald, A. Guenther, E. Kumacheva, *J. Am. Chem. Soc.* 2008, **130**, 9935; D. Dendukuri, P. S. Doyle, *Adv. Mater.* 2009, **21**, 4071; N. Prasad, J. Perumal, C. H. Choi, C. S. Lee, D. P. Kim, *Adv. Funct. Mater.* 2009, **19**, 1656; P. Panda, K. P. Yuet, T. A. Hatton, P. S. Doyle, *Langmuir* 2009, **25**, 5986; J. Park, Z. Nie, A. Kumachev, A. Abdelrahman, B. Binks, H. Stone, E. Kumacheva, *Angew. Chem.* 2009, **121**, 5404.
- 10 P. Garstecki, M. J. Fuerstman, H. A. Stone, G. M. Whitesides, *Lab Chip* 2006, **6**, 437.
- 11 D. Roper, W. Ahn, M. Hoepfner, *J. Phys. Chem.* 2007, **111**, 3636.
- 12 G. L. Liu, J. Kim, Y. Lu, L. P. Lee, *Nat. Mater.* 2006, **5**, 27; H. Chen, L. Shao, T. Ming, Z. Sun, C. Zhao, B. Yang, J. Wang, *Small* 2010, **6**, 2272.
- 13 M. Stockman, *Opt. Express* 2011, **19**, 2202, 9; B. Jankiewicz, D. Jamiola, J. Choma, M. Jaroniec, *Adv. Colloid Interface Sci.* 2012, **170**, 28; H. Chen, L. Shao, Q. Li, J. Wang, *Chem. Soc. Rev.* 2013, **42**, 2679. R. W. Conner, D. D. Dlott, *J. Phys. Chem. A* 2010, **114**, 6731; Y. Ohkura, P. M. Rao, X. Zheng, *Combust. Flame* 2011, **158**, 2544; J. E. Abboud, X. Chong, M. Zhang, Z. Zhang, N. Jiang, S. Roy, J. R. Gord, *Appl. Phys. Lett.* 2013, **102**, 023905.
- 14 C. F. Bohren, D. R. Huffman, *Absorption and Scattering of Light by Small Particles*, Wiley, New York, USA 1983.
- 15 M. F. Modest, *Radiative Heat Transfer*, Taylor & Francis Group, New York.
- 16 B. J. Lee, K. Park, T. Walsh, L. Xu, *J. Sol. Energ. Eng.* 2012, **134**, 021009.
- 17 F. J. Garcia de Abajo, A. Howie, *Phys. Rev. B* 2002, **65**, 115418; F. J. Garcia de Abajo, *Rev. Mod. Phys.* 2010, **82**, 209 and references therein; U. Hohenester, A. Trügler, *Comput. Phys. Comm.* 2012, **183**, 370.
- 18 B. Draine, P. Flatau, *J. Opt. Soc. Am. A* 1994, **11**, 1491; P. Flatau, *Opt. Lett.* 1997, **22**, 1205; M. A. Yurkin, A. G. Hoekstra, R. X. Brock, J. Q. Lu, *Opt. Express* 2007, **15**, 17902; S. Liu, J. Li, F. Zhou, L. Gan, Z.-Y. Li, *Opt. Lett.* 2011, **36**, 1296; J. Jeon, S. Park, B. J. Lee, *Opt. Express* 2014, **22**, 1413.
- 19 A. Evlyukhin, C. Reinhardt, E. Evlyukhin, B. N. Chichkov, *J. Opt. Soc. Am. B* 2013, **30**, 2589.
- 20 P. Yang, K. Liou, *J. Opt. Soc. Am. A* 1996, **13**, 2071; W. Sun, Q. Fu, *Appl. Opt.* 2000, **39**, 5569; T. Davis, K. Vernon, D. Gómez, *Opt. Express* 2009, **26**, 23655.
- 21 O. Martin, C. Girard, A. Dereux, *Phys. Rev. Lett.* 1995, **74**, 526; M. Paulus, O. Martin, *J. Opt. Soc. Am. A* 2001, **18**, 854.
- 22 S. Das, S. Choi, W. Yu, T. Pradeep, *Nanofluids: Science and Technology*, Wiley Interscience, Hoboken, NJ, USA 2008.
- 23 D. Ross, M. Gaitan, L. E. Locascio, *Anal. Chem.* 2001, **73**, 4117.
- 24 I. L. Medintz, H. T. Uyeda, E. R. Goldman, H. Mattoussi, *Nat. Mater.* 2005, **4**, 435; K. A. Kang, J. Wang, S. Achilefu, J. B. Jasinski, *J. Nanobiotech.* 2011, **9**, 1.
- 25 L. Xu, B. J. Lee, W. L. Hanson, B. Han, *Appl. Phys. Lett.* 2010, **96**, 174101; S. H. Choi, B. Kwak, B. Han, Y. L. Kim, *Opt. Express* 2012, **20**, 16785.
- 26 B. Han, W. L. Hanson, K. Bensalah, A. Tuncel, J. M. Stern, J. A. Cadeddu, *Ann. Biomed. Eng.* 2009, **37**, 1230; P. Haro-González, L. Martínez-Maestro, I. R. Martín, J. García-Solé, D. Jaque, *Small* 2012, **8**, 2652.
- 27 T. Pons, I. L. Medintz, K. E. Sapsford, S. Higashiya, A. F. Grimes, D. S. English, H. Mattoussi, *Nano Lett.* 2007, **7**, 3157; E. Dulkeith, A. Morteani, T. Niedereichholz, T. Klar, J. Feldmann, S. Levi, F. van Veggel, D. Reinhoudt, M. Möller, D. Gittins, *Phys. Rev. Lett.* 2002, **89**, 203002.
- 28 J. M. S. Bartlett, D. Stirling, *Meth. Mol. Bio.* 2003, **226**, 3.

Lab Chip

- 1
2
3
4
5
6
7
8
9
10
11
12
13
14
15
16
17
18
19
20
21
22
23
24
25
26
27
28
29
30
31
32
33
34
35
36
37
38
39
40
41
42
43
44
45
46
47
48
49
50
51
52
53
54
55
56
57
58
59
60
- 29 G. Baffou, H. Rigneault, *Am. Phys. Soc.* 2011, **84**, 1; P. H. Hoang, H. Park, D. P. Kim, *J. Am. Chem. Soc.* 2011, **133**, 14765.
30 G. Baffou, R. Quidant, C. Girard, *Phys. Rev. B* 2010, **82**, 165424.